Atom Indonesia

Journal homepage: http://atomindonesia.brin.go.id

# Carbone or Oxygen Therapy: A Comparative Dosimetric Study Using PHITS Code

**H. El Bekkouri[1*], E. Al Ibrahmi[1], M. El-Asery[1], A. Bardane[1], C. El Mahjoub[1], A. Didi[2], Z. Sadoune[1]**

[1]*Department of Physics, Faculty of Science, Ibn Tofail University, Kenitra B.P 133, Morocco*
[2]*National Energy Center of Nuclear Science and Technology (CNESTEN), B. P. 1382, R. P. 1000, Rabat, Morocco*

**ARTICLE INFO**

*Article history:*
Received 21 July 2023
Received in revised form 14 March 2024
Accepted 14 March 2024

*Keywords:*

Hadrontherapy
PHITS code
Oxygen ion
Carbon ion
Bragg curve

**ABSTRACT**

Compared to conventional radiotherapy (X-rays or γ-rays), charged particle therapy shows more potential in treating deep-seated and radio-resistant tumors. Currently, all centers that offer hadron therapy use proton or $^{12}$C ion. Ongoing research is exploring the possibility of using others heavier ions, such as oxygen ion $^{16}$O or helium ion $^{4}$He. In this study, Monte Carlo method was used employing the Particle and Heavy Ion Transport code System (PHITS), to examine the amount of dose deposited by incident particles of $^{12}$C ion with energies of 200 and 300 MeV/u, as well as $^{16}$O ions with energies of 237.5 and 358.5 MeV/u. In this study, we investigated the depth dose distribution of carbon and oxygen ion beams by comparing their energy deposition in a water phantom and the impact of secondary particles. When considering lower energies, oxygen ions are more advantageous than carbon ions as they have slightly higher peak input ratios. This property enables higher doses to be delivered to tumor targets or lower doses to healthy surrounding tissues.



## INTRODUCTION

Heavily ionized particles, such as high-energy ions or charged particles, lose energy as they pass through materials. The Bethe-Bloch equation explains the energy loss phenomenon [1], which provides a mathematical formulation of the average reduction in the amount of energy lost by a charged particle during its passage in a medium. The Bethe-Bloch equation considers various factors, including the charge and mass of the particle, its velocity, the atomic number and density of the material, and density of electrons in the medium. It provides an estimate of the energy loss due to reactions with the electrons and nuclei of the atoms in the material. As a result, there is a specific distance in the material for each charged particle to lose its energy. Ionizing radiation can be utilized to kill cancer cells, and in some cases, this therapy is necessary as 60-70 % of cancer patients require it [2]. The best way to use this therapy method is to combine its physical and radiobiological characteristics of radiation-tissue interaction [3].

Additionally, clear medical imaging of the tumor, particularly the positron emission tomography technique, is necessary for this type of treatment [4]. Charged particles have established themselves as preferred sources in radiotherapy [5] capable of providing multiple physical and radiobiological benefits over conventional radiotherapy using electron [6], proton [7], or gamma-ray therapy [8]. The biggest advantage of charged particle therapy is the deep dose distribution in the tissue, which is distinguished by a small entry dose and a rise towards the tail of the particle's trajectory in the material [9].

At the peak of the Bragg spectrum, charged particles exhibit high transfer of linear energy and increased ionization capacity, leading to enhanced relative biological efficiency. Today, various ion beams are produced by suitable accelerators. Among them, proton and carbon ion therapy are two hadronic therapies that are increasingly being utilized to treat cancer. Due to their superior radiobiological performance, decreased lateral scattering, and high linear energy transfer compared to carbon ions, oxygen ions are now viewed as potential replacements for carbon ions, given their mass [10]. This translates to better treatment

*Corresponding author.
E-mail address: hassane.elbekkouri@uit.ac.ma
DOI: https://doi.org/10.55981/aij.2024.1352

efficiency for hypoxic tumors. In 2012, Kurz et al. carried out the first scientific investigations into the interaction of a beam of oxygen ions with matter [11].

This study presents a comparison between depth dose distributions of $^{16}O$ ions measured at the HIT (Heidelberg Ion-Beam Therapy Center) and simulated using the Monte Carlo code Fluka. It focuses on determining the positions of the Bragg peak and understanding the factors affecting the distribution shapes. Their work has created a database of preliminary oxygen beam tests to support experiments on the radiobiology of oxygen beams. To our knowledge, there are few studies that describe in greater detail the comparison between the use of carbon and oxygen ions to treat tumors. With this in view, this study was carried out using the Monte Carlo method, given the absence of experimental results.

The study utilizes the Monte Carlo simulation method with the PHITS (Particle and Heavy-Ion Transport Code System) code to compare the doses generated by an oxygen ion beam ($^{16}O$) and a carbon ion beam ($^{12}C$) in a water phantom.

PHITS is a comprehensive particle transport simulation software that incorporates various nuclear reaction models and datasets [12]. It can handle the transport of most particle types with energies up to 1 TeV/u (per nucleon for ions). The latest version (3.32) of PHITS utilizes the Kurotama reaction cross-section mode [13] and JAERI Quantum Molecular Dynamics (JQMD) version 2 to calculate nuclear reactions between heavy ions [14]. For both the evaporation of light particles and the fission of excited remaining nuclei, the generalized evaporation model (GEM-2.0) [15] was utilized. The Event Generator Mode has been incorporated into the PHITS code to assess how deposit energy is distributed below 20 MeV. The interactions between electrons, positrons, and photons at the atomic level were simulated using the EGS5 [16] algorithm. Used in the input file (nspred = 2 and nedisp = 1) [17], charged particles' angular and energetic straggling was taken into consideration. Using the ATIMA [18] code, the energy losses of charged particles other than electrons and positrons were estimated. For simulating nuclear and atomic collisions, the physical models and data libraries that are advised for usage in PHITS-3.32 are explicitly in reference [19].

## METHODOLOGY

The use of Monte Carlo simulation, which provides a solid tool for the numerical computation of stochastic occurrences, has substantially helped the research of radiation-matter interactions. In situations where doing trials is either impossible or impractical, it enables the presentation of extremely exact information. At present, recognized general-purpose codes like Geant4 [20], FLUKA [21,22], MCNPX [23], PHITS [12], and Shield-HIT [24] are employed for carbon ion treatment applications. They were all initially created for high-energy physics.

The geometry employed in this study is a typical phantom that has a radius of 10 cm, is constrained by two planes at the Z axis (0 and 40 cm), and is centered inside a sphere with a radius of 500 cm (Fig. 1.). The parameters used were chosen to correspond to those of a sample tumor. A 1 cm diameter cylinder outside at 20 cm serves as the ions beam's source, exposing the phantom along the horizontal z-axis. In the simulation parameters, we have adopted $10^6$ as the main number of stories to obtain a good relative error.

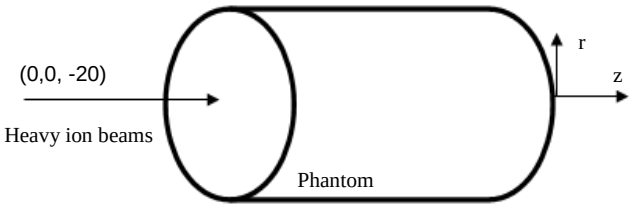


**Fig. 1.** The geometry used for the simulation.

## RESULTS AND DISCUSSION

### $^{12}C$ and $^{16}O$ bragg curves

To verify the ability of PHITS to simulate linear energy transfer phenomena [25], a comparison between the simulation results and experimental data was conducted. The experimental data were obtained from the NASA Space Radiation Laboratory website [26] which is operated by the U.S. Department of Energy. The information concerns carbon and oxygen beams propagated through a high-density polyethylene (HDPE) phantom with a density of 0.97 $g.cm^{-3}$ and energies of 200.2 MeV/u and 284.1 MeV/u, respectively. The energies of $^{12}C$ and $^{16}O$ ions beams were chosen to be 200.2 MeV/u and 284.1 MeV/u respectively, because in the database of Bragg peak measurements at the NASA Space Radiation Laboratory, there are two energies (200.2 MeV/u and 292.7 MeV/u) for carbon ions and two for oxygen ions (284.1 MeV/u and 594.4 MeV/u). To avoid duplicating work, we chose 200.2 for $^{12}C$ and 284.1 for $^{16}O$. Simulations have been carried out for the other two energies, showing good similarity between experiment and simulation. It is clear from Fig. 2 that PHITS closely mimics the experimental Bragg curve.

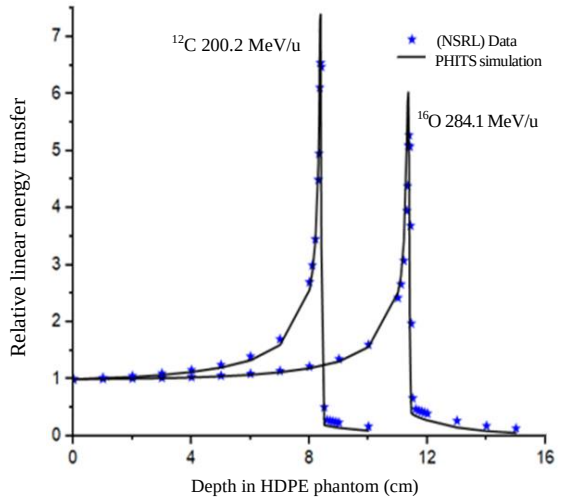


**Fig. 2**. PHITS-simulated and measured Bragg curves at energies of 200.2 MeV/u for $^{12}$C and 284.1 MeV/u for $^{16}$O. Statistical uncertainties are under 0.4 %.

## Depth-dose distribution of $^{12}$C and $^{16}$O ion beams in a water phantom

The most crucial factor to research for cancer treatment is the depth dose supplied by charged particles penetrating the tissue. To investigate this qualitatively, a $^{12}$C ion beam at 200 MeV/u and a $^{16}$O ion beam at 237.5 MeV/u (both energies having the same Bragg peak at approximately 8.67 cm) were simulated in a water phantom.

Figure 3 illustrates the energy stored in each incoming particle within the phantom for cases involving 200 MeV/u for $^{12}$C and 237.5 MeV/u for $^{16}$O. The figure demonstrates that the $^{16}$O beam deposits approximately 58 % more energy than the $^{12}$C beam at a depth of 0.4 cm inside the phantom. Moreover, at the Bragg peak, the $^{16}$O beam deposits around 66 % more energy compared to the $^{12}$C beam. This difference in energy deposition arises from the higher mass of $^{16}$O ions compared to $^{12}$C ions, as the energy deposited by the ion is influenced by various factors outlined in the Bethe-Bloch formula, primarily its velocity and mass. Beyond the Bragg peak, the $^{16}$O beam exhibits a more pronounced energy tail. The peak-to-input ratio is calculated to be 7.83 for $^{16}$O and 7.46 for $^{12}$C.

Figure 4 depicts the energy deposited within the phantom for a 300 MeV/u $^{12}$C beam and a 358.5 MeV/u $^{16}$O beam, respectively. The data presented in this figure indicate that at a depth of 0.4 cm into the phantom, the $^{16}$O beam results in approximately 60 % more energy deposition than the $^{12}$C beam. Similarly, at the Bragg peak, the $^{16}$O beam yields approximately 59 % more energy deposition compared to the $^{12}$C ion beam. However, the $^{16}$O beam demonstrates a higher energy tail after the Bragg peak. The peak-to-input ratio for the $^{16}$O beam and the $^{12}$C beam is calculated to be 4.75 and 4.79, respectively.

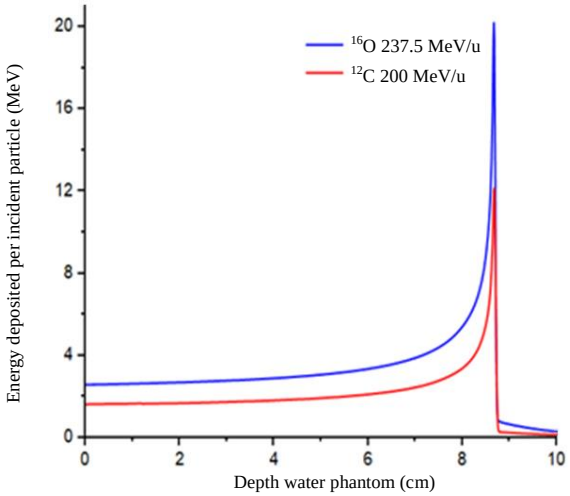


**Fig. 3.** Comparison of the energy deposition rates for 200 MeV/u of $^{12}$C and 237.5 MeV/u of $^{16}$O in a water phantom.

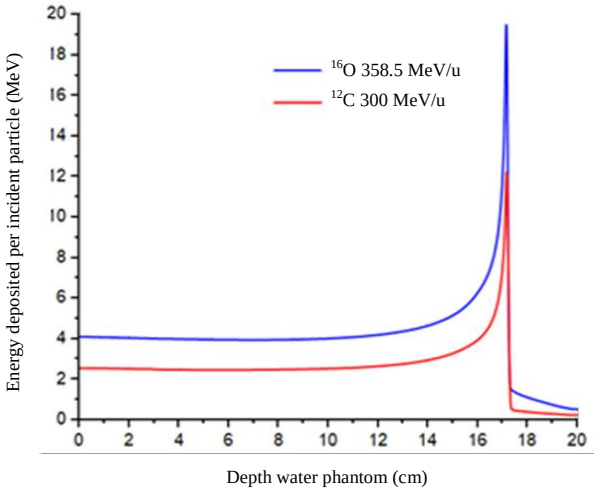


**Fig. 4.** Comparison of energy deposition in a water phantom for 300 MeV/u of $^{12}$C and 358.5 MeV/u of $^{16}$O.

The use of oxygen beams yields a slightly higher dose per incident ion compared to carbon beams. The presence of a tail in the deposition of dose can be attributed to the occurrence of nuclear fragmentation processes that take place when the primary ion beam interacts with the atoms of the irradiated water phantom. This variation in the distribution of dose has the potential to affect the intended dose delivered to both the tumor and the surrounding healthy tissues, thus increasing the probability of unwanted side effects and complications. As a result, careful consideration must be given to treatment planning and optimization to maximize the effectiveness of therapy while minimizing risks to healthy tissues.

These findings indicate that a higher peak-to-input ratio implies the potential for modifying the dose delivered to the tumor target while affecting healthy tissues surrounding the tumor site. The study reveals that the peak-entry ratio for both oxygen and carbon ions decreases as the beam energy increases. Additionally, it is observed that oxygen ions offer greater advantages in terms of peak-to-input ratio at lower energies.

## Spatial distribution of the flux of $^{16}O$ and $^{12}C$

To demonstrate the lateral and longitudinal beam spread, which represents the spatial distribution of the flux of $^{12}C$ and $^{16}O$ ions beams in a water phantom, we conducted a 2D simulation. The simulation was performed at an energy of 300 MeV/u for $^{12}C$ ions and 358.5 MeV/u for $^{16}O$ ions. The obtained results are depicted in Figs. 5 (a) and (b).

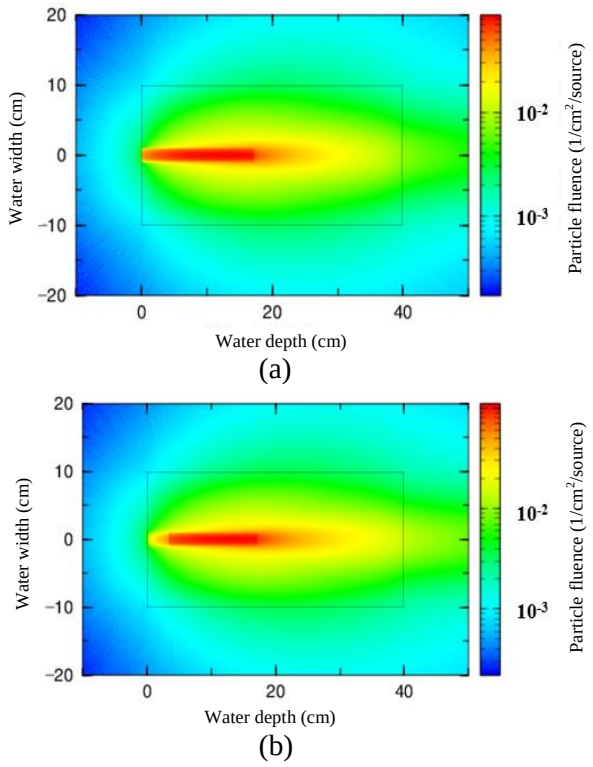


**Fig. 5.** (2D) Particle fluence inside and around the water phantom for the energy of 300 MeV/u for $^{12}C$ (a) and 358.5 MeV/u for $^{16}O$ (b).

When an ion beam passes through matter, the particles undergo elastic Coulomb interactions with the target nuclei and atomic electrons. As a result of these interactions, the direction of the particle changes from the original direction. The size of the lateral scattering is related to the density of the target material and the weight of the primary particle. The higher the material density, the more scattering events occur, resulting in a larger lateral dispersion of the beam. At the same time, a heavier particle will experience less deviation from its initial direction than lighter particles. If we consider a carbon beam and an oxygen beam with respective energies of 300 MeV/u and 358.5 MeV/u, both passing through a volume of water, we can observe from Fig. 5 that the oxygen beam shows less lateral dispersion than the carbon beam.

## Depth-dose distribution of secondary particles of $^{12}C$ and $^{16}O$ ions

Estimating the dose for secondary particles, such as neutrons, poses a greater challenge due to the Bragg curve representing the total dose of all particles. In this study, we conducted simulations to assess the dose contribution of secondary particles from a $^{16}O$ ion beam with incident energies of 358.5 MeV/u and 300 MeV/u for $^{12}C$ in a water phantom using the PHITS Monte Carlo Code.

Figure 6 illustrates the energy deposited by the secondary particle field generated by incident carbon ions at an energy of 300 MeV/u and oxygen ions at 358.5 MeV/u across the depth of the phantom. The results demonstrate that fragmentation plays a more significant role in the case of oxygen beams in the plateau region, at the location of the Bragg peak, and beyond. Specifically, the contribution of carbon ion fragments is approximately 44 % smaller than that of oxygen ions. The energy distribution of secondary particles has been extensively investigated in several articles, including "Monte Carlo simulation for calculation of fragments produced by a 400 MeV/u carbon ion beam in water" for $^{12}C$ [27] and "Elemental fragmentation cross sections for a 400 MeV/u oxygen-16 beam interacting with a graphite target using the FOOT ΔE-TOF detectors" for $^{16}O$ [28].

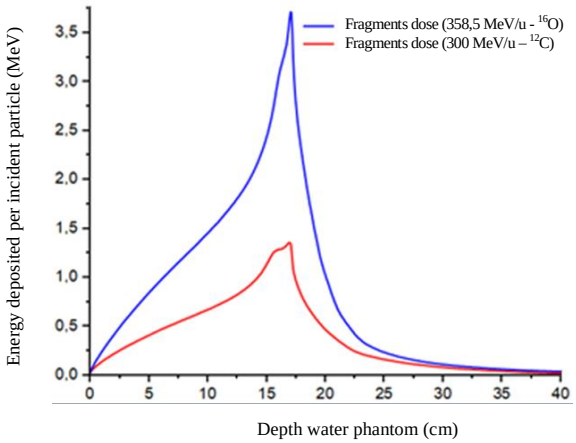


**Fig. 6**. Comparison of the energy deposited by the secondary particles of two ion beams, carbon, and oxygen.

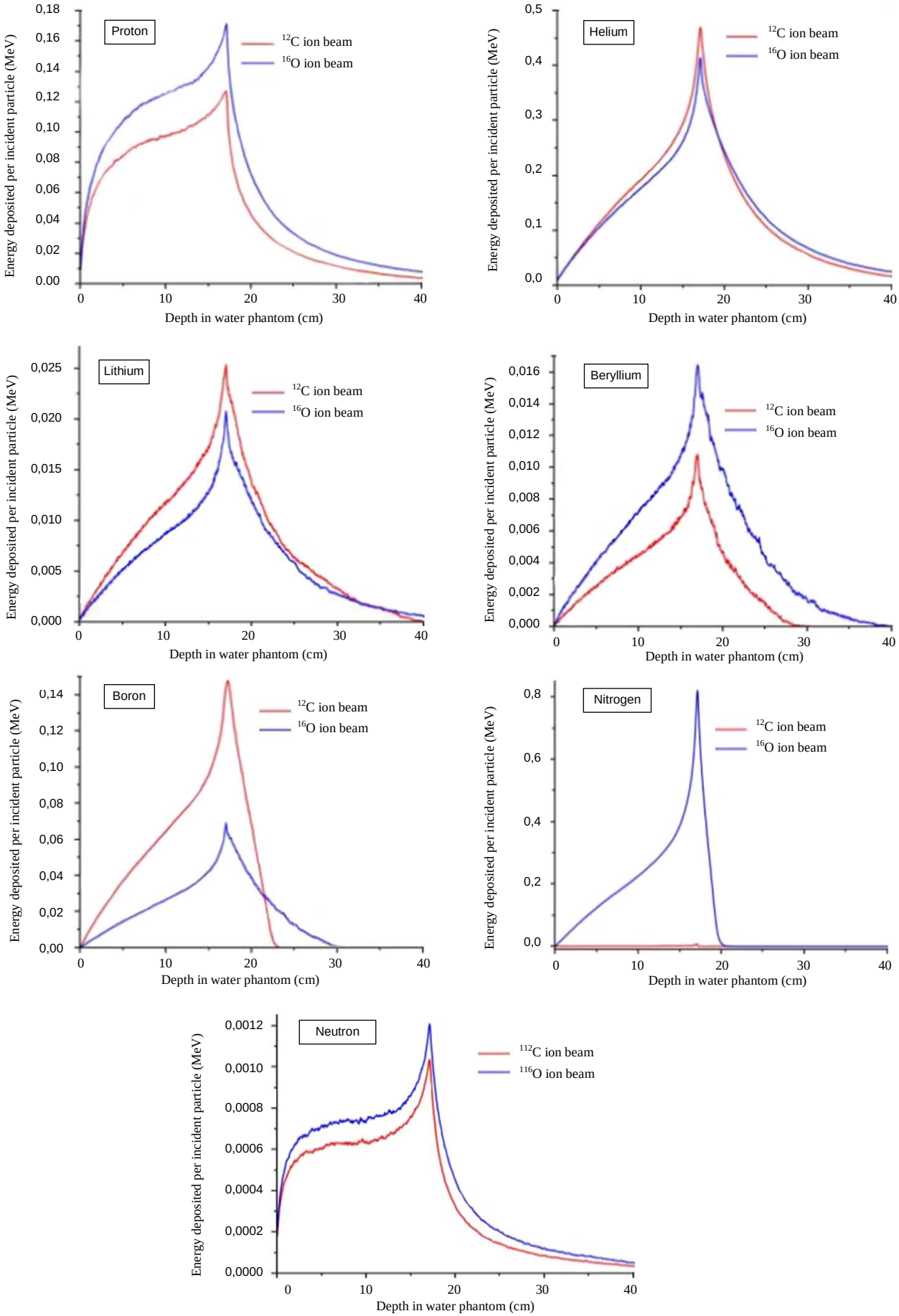


**Fig. 7**. Comparison of depth-energy deposition curves for certain fragment species, with oxygen and carbon ion beams at energies of 385.5 MeV/u and 300 MeV/u, respectively.

Figure 7 presents a detailed comparison of the contributions of fragment particles from both carbon and oxygen ion beams. Hydrogen and helium fragments exhibit a greater range compared to incident ions and heavier fragments, making them the primary contributors to the dose beyond the Bragg peak. The energy deposition of secondary protons generated by oxygen ion beams surpasses that of carbon ion beams across all regions. Both oxygen and carbon ion beams demonstrate similar contributions of secondary alpha particles to energy deposition along the Bragg peak, but oxygen ions result in higher energy deposition by alpha particles after the Bragg peak.

Secondary lithium and boron fragments yield higher doses than oxygen ions in the plateau region and at the Bragg peak position when utilizing carbon ion beams. However, the addition of oxygen ions enhances the dose contribution of these particles after the Bragg peak. In contrast to carbon ion beams, beryllium contributes more in all areas when oxygen ion beams are employed. Throughout the Bragg peak region, secondary nitrogen fragments, resulting from primary oxygen ions, contribute the most to energy deposition. The influence of neutrons is most pronounced when utilizing oxygen ion beams in all regions, including the plateau region, the Bragg peak position, and beyond.

These findings align with the work of C.K. Ying et al. conducted using the Geant4 simulation code [29].

Considering this study and other related studies [30,31], where the authors demonstrated the biological properties and effects of oxygen compared to protons, as well as the fact that Intensity Modulated Proton Therapy (IMPT) offers a greater dose reduction than Intensity Modulated Radiation Therapy (IMRT), thereby reducing off-target doses, it can be concluded that oxygen ions may be a suitable option for treating radio-resistant tumors located deeper within the body while minimizing damage to surrounding tissues.

## CONCLUSION

In this study, we explored the depth dose distribution of carbon ion and oxygen ion beams by comparing the energy deposition they produced in a water phantom. Our findings revealed that oxygen beams resulted in a higher dose and a greater peak-to-input ratio when compared to carbon ion beams. According to this study, oxygen ion therapy is more efficient than carbon ion therapy in terms of dose deposition at the BP level. However, oxygen ion beams are known to produce more nuclear fragments that deposit energy on the opposite side of the BP.

## ACKNOWLEDGMENT

The Japan Atomic Energy Agency (JAEA)'s Center for Computational Science & e-Systems Director granted the authors permission to utilize the Particle and Heavy Ion Transport System (PHITS) code, which the authors are grateful for. We particularly appreciate the conversations that the scientists from the Materials and Subatomic Physics Laboratory provided.

## AUTHOR CONTRIBUTION

The main authors of this study were H. El Bekkouri and E. Al Ibrahmi, who each contributed equally. The final draft of the manuscript was read and approved by all authors.

## REFERENCES

1. H. Bethe, Ann. Phys. **397** (1930) 325.
2. V. Raj, A. Rai, S. Sharma *et al*., J. Anal. Pharm. Res. **7** (2018) 175.
3. J. E. Scaife, G. C. Barnett, D. J. Noble *et al*., Br. J. Radiol. **88** (2015) 20150172.
4. A. Bardane, J. Tajmouaati and A. Maghnouj, Moscow University Physics Bulletin **75** (2020) 58.
5. A. Boukhellout, N. Ounoughi and F. Kharfi, Radiat. Prot. Dosimetry **198** (2022) 31.
6. A. Khorshidi, A. Rajaee, M. Ahmadinejad *et al.* Phys. Scr. **89** (2014) 095001.
7. P. Azimi and A. Movafeghi, International Clinical Neuroscience Journal **3** (2016) 59.
8. J. S. Nabipour and A. Khorshidi, J. Med. Imaging Radiat. Sci. **49** (2018) 194.
9. U. Amaldi and G. Kraft, Reports on Progress in Physics **68** (2005) 1861.
10. I. Kantemiris, E. P. Pappas, G. Lymperopoulou *et al.*, J. Pers. Med. **13** (2022) 1.
11. C. Kurz, A. Mairani and K. Parodi, Phys. Med. Biol. **57** (2012) 5017.
12. T. Sato, Y. Iwamoto, S. Hashimoto *et al*., J. Nucl. Sci. Technol. **55** (2018) 684.
13. K. Iida, A. Kohama and K. Oyamatsu, J. Phys. Soc. Jpn. **76** (2007) 44201.
14. T. Ogawa, T. Sato, S. Hashimoto *et al.*, Phys. Rev. C **92** (2015) 24614.

15. S. Furihata, *The GEM Code - the Generalized Evaporation Model and the Fission Model*, in: Advanced Monte Carlo for Radiation Physics, (2001) 1045.
16. H. Hirayama, Y. Namito, A. F. Bielajew *et al.*, The EGS5 Code System, 1-1 Oho, Tsukuba-shi Ibaraki-ken, Japan (2005).
17. N. Ounoughi, Y. Dribi, A. Boukhellout *et al.*, Pol. J. Med. Phys. Eng. **28** (2022) 160.
18. H. Weick, H. Geissel N. Iwasa *et al.*, GSI Scientific Report (2017) 2011.
19. D. Satoh and T. Sato, J. Nucl. Sci. Technol. **59** (2022) 1047.
20. S. Agostinelli, J. Allison, K.Amako *et al.*, Nucl. Instrum. Methods Phys. Res. A **506** (2003) 250.
21. A. Ferrari P. R. Sala and A. Fasso *et al.*, CERN-2005-010, INFN-TC-2005-11, SLAC-R-773, CERN-2005-10 (2005).
22. G. Battistoni, F. Cerutti, A. Fasso *et al.*, *The FLUKA Code: Description and Benchmarking*, AIP Conf. Proc. **896** (2007) 31.
23. L. S. Waters, G. W. McKinney, J. W. Durkee *et al*., AIP Conf. Proc. **896** (2007) 81.
24. A. V Dementyev, N. M. Sobolevsky, Radiat. Meas. **30** (1999) 553.
25. T. D. Malouff, A. Mahajan, S. Krishnan *et al*., Front. Oncol. **10** (2020) 82.
26 Anonymous, NASA Space Radiation Laboratory. https://www.bnl.gov/nsrl/userguide/bragg-curves-and-peaks.php. Retrieved in March (2023).
27. H. F. Ou, B. Zhang and S. J. Zhao, Nucl. Instrum. Methods Phys. Res. B **396** (2017) 1825.
28. M. Toppi, A. Sarti, A. Alexandrov *et al*., Front. Phys. 10 (2022) 1.
29. C. K. Ying, D. Bolst, A. Rosenfeld *et al.*, J. Med. Phys. **44** (2019) 263.
30. L. Rezaee, Razi J. Med. Sci. **25** (2019) 85
31. V. Vernanda, A. Azzi, S. A. Pawiro, Atom Indones. **49** (2023) 7.